

Angewandte Chemie

Eine Zeitschrift der Gesellschaft Deutscher Chemiker

GDCh

www.angewandte.de

Akzeptierter Artikel

Titel: Divalent Titanium via Reductive N-C Coupling of a TiIV Nitrido with π -Acids.

Autoren: Mrinal Bhunia, Christian Sandoval-Pauker, Dominik Fehn, Lauren Grant, Shuruthi Senthil, Michael Gau, Andrew Ozarowski, Jurek Krzystek, Joshua Telser, Balazs Pinter, Karsten Meyer, and Daniel J. Mindiola

Dieser Beitrag wurde nach Begutachtung und Überarbeitung sofort als "akzeptierter Artikel" (Accepted Article; AA) publiziert. Die deutsche Übersetzung wird gemeinsam mit der endgültigen englischen Fassung erscheinen. Die endgültige englische Fassung (Version of Record) wird ehestmöglich nach dem Redigieren und einem Korrekturgang als Early-View-Beitrag erscheinen und kann sich naturgemäß von der AA-Fassung unterscheiden. Leser sollten daher die endgültige Fassung, sobald sie veröffentlicht ist, verwenden. Für die AA-Fassung trägt der Autor die alleinige Verantwortung.

Zitierweise: *Angew. Chem. Int. Ed.* **2024**, e202404601

Link zur VoR: <https://doi.org/10.1002/anie.202404601>

RESEARCH ARTICLE

Ti^{II} via Reductive N-C Coupling of a Ti^{IV} Nitrido with π -Acids.

Mrinal Bhunia,^a Christian Sandoval-Pauker,^b Dominik Fehn,^c Lauren N. Grant,^a Shuruthi Senthil,^a Michael R. Gau,^a Andrew Ozarowski,^d J. Krzystek,^d Joshua Telser,^{*,e} Balazs Pinter,^{*,b} Karsten Meyer,^{*,c} and Daniel J. Mindiola^{*,a}

Dedicated to Professor Peter T. Wolczanski on the occasion of his 70th birthday.

Abstract: The nitrido-ate complex $[(\text{PN})_2\text{Ti}(\text{N})\{\mu_2\text{-K}(\text{OEt}_2)\}]_2$ (1) ($\text{PN}^- = (\text{N}-(2\text{-P}^{\text{Pr}}_2\text{-4-methylphenyl})-2,4,6\text{-Me}_3\text{C}_6\text{H}_2)$) reductively couples CO and isocyanides in the presence of DME or cryptand, to form rare, five-coordinate Ti^{II} complexes having a linear cumulene motif, $[\text{K}(\text{L})][(\text{PN})_2\text{Ti}(\text{NCE})]$ ($\text{E} = \text{O}$, $\text{L} = \text{Kryptofix}222$, (2); $\text{E} = \text{NAd}$, $\text{L} = 3$ DME, (3); $\text{E} = \text{N}^{\text{t}}\text{Bu}$, $\text{L} = 3$ DME, (4); $\text{E} = \text{NAd}$, $\text{L} = \text{Kryptofix}222$, (5)). Oxidation of **2-5** with $[\text{Fc}^*][\text{OTf}]$ afforded an isostructural Ti^{III} center containing a neutral cumulene, $[(\text{PN})_2\text{Ti}(\text{NCE})]$ ($\text{E} = \text{O}$, (6); $\text{E} = \text{NAd}$ (7), $\text{N}^{\text{t}}\text{Bu}$ (8)) and characterization by CW X-band EPR spectroscopy, revealed unpaired electron to be metal centric. Moreover, 1e⁻ reduction of **6** and **7** in the presence of cryptand cleanly reformed corresponding discrete Ti^{II} complexes **2** and **5**, which were further characterized by solution magnetization measurements and high-frequency and -field EPR (HFEPR) spectroscopy. Furthermore, oxidation of **7** with $[\text{Fc}^*][\text{B}(\text{C}_6\text{F}_5)_4]$ resulted in a ligand disproportionated Ti^{IV} complex having *transoid* carbodiimides, $[(\text{PN})_2\text{Ti}(\text{NCNAd})_2]$ (9). Comparison of spectroscopic, structural, and computational data for the divalent, trivalent, and tetravalent systems, including their ¹⁵N enriched isotopomers demonstrate these cumulenes to decrease in order of backbonding as $\text{Ti}^{\text{II}} \rightarrow \text{Ti}^{\text{III}} \rightarrow \text{Ti}^{\text{IV}}$ and increasing order of π -donation as $\text{Ti}^{\text{II}} \rightarrow \text{Ti}^{\text{III}} \rightarrow \text{Ti}^{\text{IV}}$, thus displaying more covalency in Ti^{III} species. Lastly, we show a synthetic cycle whereby complex **1** can deliver an N-atom to CO and CNAd.

Introduction

Transition-metal nitrides play a key role in the formation of N-C bonds in value-added compounds such as amino acids, pharmaceuticals, agrochemicals, and heteroaromatics.¹ One of

the most attractive strategies for N-C bond formation is N-atom transfer to alkenes,² dienes,³ carbenes,⁴ CO,⁵ isocyanides,^{5b,5c,6} and cyclic or conjugated olefins.^{1d,7} Considering their rich application in a myriad of disciplines, including materials science and surface chemistry, the isolation of molecular early-transition metal nitrides has garnered considerable interest.^{8,9} Unfortunately, the proclivity of early-transition metal nitrides to bridge or oligomerize precludes their extensive reactivity studies.^{10,11} Although early-transition metal nitrides are nucleophilic at the N-center and exhibit reactivity with various electrophiles,^{12,13} reductive N-C coupling with π -acids, such as CO and isocyanides, has been underexplored, despite the utility of the resulting new N-C coupled products in organic synthesis.^{19,5a-5d} Moreover, the stabilization and concurrent reactivity study of the resulting low-valent metal complexes having functionalized nitrogenated substrates through reductive coupling is highly promising.

Intrigued by the scarce examples of molecular and terminal group 4 metal nitrides,^{14,15} we sought to explore the reductive N-C coupling of titanium nitride as systematic studies of its reactivity are largely unknown. Recently, we reported molecular terminal titanium nitrides,^{14b} which are nucleophilic at the nitrido N-atom.¹⁶ However, what would one expect if a nucleophilic titanium nitride were treated with π -acids such as carbon monoxide or an isonitrile? In this regard, Cummins (using CO) and Kawaguchi (using CO and CNxylyl, xylyl = 2,6-Me₂C₆H₃) have shown the reaction with group 5 transition metals such as a vanadium nitride anion $[\text{L}_3\text{V}\equiv\text{N}]^-$ ($\text{L} = \text{N}^{\text{t}}\text{Bu}[\text{Ar}]$, $\text{Ar} = 3,5\text{-Me}_2\text{C}_6\text{H}_3$; $\text{L}_3 = 2,6\text{-}(3\text{-}^{\text{t}}\text{Bu}-5\text{-Me}-2\text{-OC}_6\text{H}_2\text{CH}_2\text{-}4\text{-}^{\text{t}}\text{Bu-(}p\text{-tolyl)}\text{NC}_6\text{H}_4)$ to produce three-coordinate V^{III} species, L_3V , along with the liberation of cyanate (reaction with CO is shown in top of Scheme 1).^{5a,5c} Notably, Kawaguchi found that a vanadium nitride, derived from reductive splitting of N₂, can react with both CO or CNxylyl to form anionic V^{III} species having a bound cumulene and its subsequent displacement in the case of cyanate could be achieved by addition of a stronger π -acid such as 2-butyne.^{5c} This result suggested the cumulene to be weakly bound to the V^{III} ion. However, a different scenario has been witnessed by Cummins wherein the V^{V} nitride anion $[\text{L}_3\text{V}\equiv\text{N}]^-$ ($\text{L} = \text{N}^{\text{t}}\text{Bu}[\text{Ar}]$) reductively couples with CO, thus generating free cyanate salt and an open coordination site around the V-center.^{5a} When examining Nb, Cummins found that the cyanate ligand undergoes reductive cleavage to yield an Nb nitride anion, presumably *via* a putative and highly reducing $\text{Nb}^{\text{II}}\text{-cyanate}$ salt (top right, Scheme 1).^{13f} In these cases, the d² cyanate species $[\text{L}_3\text{M}(\text{NCO})]^-$ ($\text{M} = \text{V}$, Nb) appear to share common intermediates *en route* to N-C bond formation or splitting, respectively. Given the diagonal relationship between Ti and Nb and the fact that Ti^{II} is a stronger reducing agent than isoelectronic V^{V} , one would anticipate the microscopic reverse step to be more favorable: Reductive decarbonylation of a

[*] M. Bhunia, L. N. Grant, S. Senthil, M. R. Gau, Prof. Dr. D. J. Mindiola

Department of Chemistry, University of Pennsylvania
Philadelphia, PA 19104, USA

E-mail: mindiola@sas.upenn.edu

C. S. Pauker, Prof. Dr. B. Pinter[§]

Department of Chemistry and Biochemistry, University of Texas at El Paso, El Paso, TX 79968, USA
E-mail: bpinter@utep.edu

D. Fehn, Prof. Dr. Karsten Meyer

Inorganic Chemistry, Department of Chemistry and Pharmacy, Friedrich-Alexander-University Erlangen-Nürnberg (FAU), 91058 Erlangen, Germany

Email: karsten.meyer@fau.de

Dr. A. Ozarowski, Dr. J. Krzystek

National High Magnetic Field Laboratory, Florida State University, Tallahassee, Florida 32310, USA
Prof. Dr. Joshua Telser

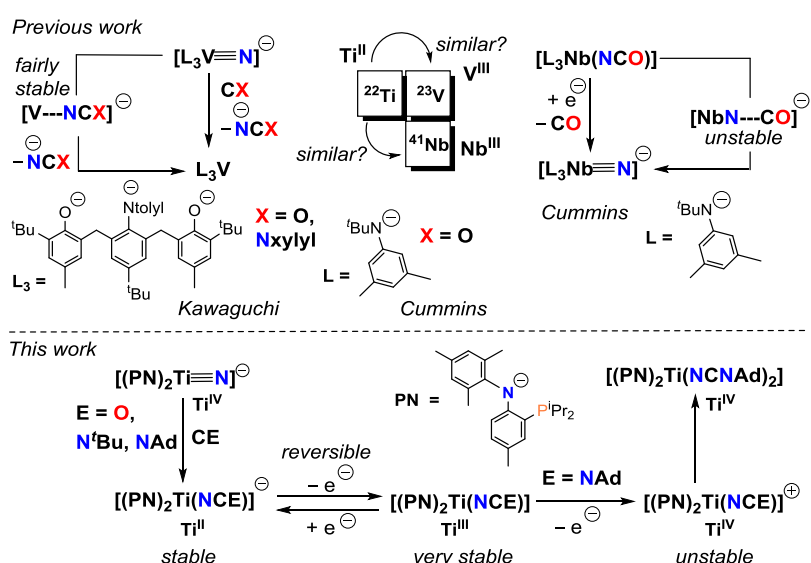
Department of Biological, Physical and Health Sciences, Roosevelt University, Chicago, Illinois 60605, USA

Email: jtelsler@roosevelt.edu

Supporting information for this article is given via a link at the end of the document.

[§] Current affiliation: European Research Council Executive Agency. Disclaimer: The views expressed are purely those of the authors and may not in any circumstances be regarded as stating an official position of the ERCEA and the European Commission.

RESEARCH ARTICLE



Scheme 1. (Top left) Cyanate elimination from CO and the V nitride anion, (top middle) State-of-the-art, and (top right) reductive decarbonylation of an isoelectronic Nb(NCO) anion to the nitride anion (center). (Bottom) Our current work involving reductive coupling of a Ti nitride with CO, CNAd, and CN⁺Bu, and subsequent redox chemistry by 1 or 2 e⁻.

transient Ti^{II} isocyanate anion to form CO and the titanium nitride anion is akin to the behavior of an isoelectronic Nb^{III} fragment (top right, Scheme 1). However, Kawaguchi's isolation of discrete cumulene salts $[\text{L}_3\text{V}(\text{NCO})]^-$ and $[\text{L}_3\text{V}(\text{NCNxylyl})]^-$ suggested that 3d metal systems, including isovalent Ti^{II} , could be likewise assembled directly from a high-valent nitride precursor.

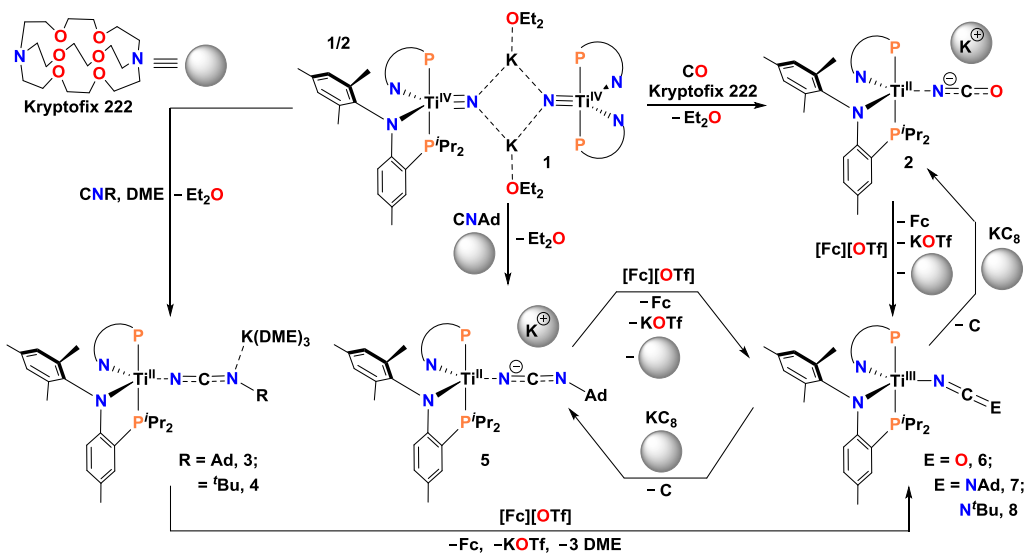
Inspired by Cummins and Kawaguchi, we show in this study how an anionic titanium nitride moiety reacts with CE ($E = O$ or NR ; $R = 'Bu$, Ad) to form rare examples of anionic Ti^{II} -ate or discrete Ti^{II} salt complexes containing the cumulenes NCO (cyanate) or $NCNR$ (cyanamide). Our work demonstrates that the nitride group in Ti behaves more in line with the V chemistry shown in Scheme 1, akin to what Kawaguchi described. Notably,

we show how 5-coordinate Ti^{II} compounds can be assembled and how sequential one- and two-electron oxidation of the Ti^{II} species yields Ti^{III} and Ti^{IV} complexes possessing linear and terminal NCE motifs with notable changes in the Ti –NCE bonding topology (bottom, Scheme 1). Although the titanium nitride can be regarded as highly nucleophilic, the transformations described here involve 2 e^- reactivity with the nitride ligand serving as a conduit for electron transfer from the substrate (CE) to the Ti center. A combination of structural, spectroscopic (IR, HFEPR, CW X-band EPR), electrochemical and synthetic redox studies, isotopic labeling experiments, and computational studies are provided for these rare examples of Ti^{II} , Ti^{III} , and even Ti^{IV} systems supporting cumulenes such as NCE. Moreover, we also describe a synthetic cycle involving a Ti^{IV} nitrido complex and its reductive coupling with CE.

Results and Discussion

Construction and Structural Identification of Cyanate and Carbodiimide Adducts Bound to Divalent Titanium. The

carboxamides Adducts Bound to Divalent Titanium. The titanium nitride anion complex $[(PN)_2Ti(N\{ \mu_2-K(OEt_2)\})_2]$ (**1**) ($PN^- = N(2-P^iPr_2-4\text{-methylphenyl})-2,4,6\text{-Me}_3C_6H_2$) has been shown to be a potent nucleophile and readily forms imide complexes when treated with various electrophiles.¹⁶ Likewise, the nitride nitrogen of **1** is quite basic and can deprotonate the amine $HN\{Si(CH_3)_3\}_2$ (pK_a of 25.8 in *thf* at 25 °C) but not HN^+Pr_2 (pK_a of 36 in *thf* at 25 °C).¹⁶ Since complex **1** can readily deoxygenate $CIC(O)^+Bu$ or $OCCPPh_2$ and completely transfer the nitrido nitrogen, we explored its reactivity with CO in hopes of mimicking chemistry reported by Cummins and Kawaguchi (vide supra, Scheme 1). However, one could also anticipate no reaction taking place given



Scheme 2. Synthesis of Ti^{II} complexes **2-5** from CO and CNR (R = ^tBu , Ad) addition to the nitride salt **1**. Oxidation of **2-5** to form corresponding neutral Ti^{III} complexes **6-8**. One-electron reduction of the Ti^{III} complexes **6** and **7** to their corresponding Ti^{II} analogs are also depicted.

RESEARCH ARTICLE

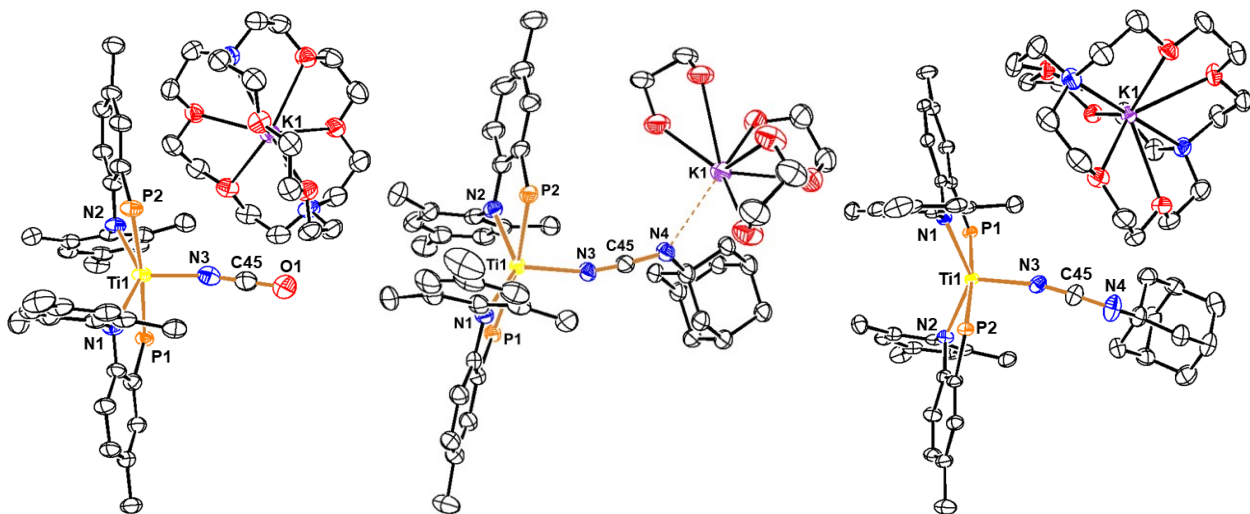


Figure 1. Molecular structures of the Ti^{II} complexes **2** (left), **3** (middle), and **5** (right) with thermal ellipsoids at the 50% probability level.¹⁸ Residual solvent molecules and hydrogen atoms are omitted for clarity. The structure of **4** is shown in the SI.

the diagonal relationship between Ti and Nb akin to what Cummins reported for Nb (vide supra, top right of Scheme 1).^{13f} To our initial attempt, treatment of **1** with 1 atm of CO in thf resulted in an immediate reaction but with the formation of a mixture of species.¹⁷ However, when conducting the same reaction in the presence of cryptand, Kryptofix222 (4,7,13,16,21,24-hexaoxa-1,10-diazabicyclo[8.8.8]hexacosane), we were fortunate to isolate, albeit in moderate yield (34%), the Ti^{II} cyanate salt $[\text{K}(\text{cryptand})][\text{(PN)}_2\text{Ti}(\text{NCO})]$ (**2**) based on single crystal X-ray diffraction (scXRD) and IR spectroscopic study as shown on the left of Figure 1 and Scheme 2. The scXRD of **2** provided crucial structural information by revealing C–N bond formation between CO and the nitrido nitrogen of **1** to yield an example of a rare five-coordinate Ti^{II} -isocyanate complex confined to a trigonal bipyramidal geometry ($\tau_5 = 0.711$). The structure of **2** also shows *transoid* phosphino groups ($\text{P}-\text{Ti}-\text{P}$, 175.13(4) $^{\circ}$) and a fairly linear topology for the $\text{Ti}-\text{NCO}$ linkage ($\text{Ti}-\text{N}-\text{C}$, 172.3(4); $\text{N}-\text{C}-\text{O}$, 179.7(6) $^{\circ}$). Formation of cyanate results in significant elongation of the $\text{Ti}-\text{N}$ (2.102(4) \AA) when compared to the extremely short $\text{Ti}\equiv\text{N}$ bond in **1** (1.660(2) \AA).^{14b} Table 1 shows salient metrical parameters for **2**, wherein $\text{N}-\text{C}$ (1.170(6) \AA)¹⁹ and $\text{C}-\text{O}$ (1.214(6) \AA)^{5h} distances within the linear NCO-fragment ($\angle \text{N}-\text{C}-\text{O} = 179.7(6)^{\circ}$) support likely triple and single bonding, respectively. Additionally, a long $\text{Ti}-\text{N}$ (2.102(4)

\AA) distance is in good agreement with weakly bound cyanate with Ti^{II} . An IR spectrum of **2** manifests a strong stretch for the bound cyanate ligand at 2196 cm^{-1} , which was irrefutably assigned by preparing the isotopically ^{15}N enriched isotopomer $[\text{K}(\text{cryptand})][\text{(PN)}_2\text{Ti}(\text{NCO})]$ (**2**- ^{15}N) from 50% ^{15}N enriched **1**- ^{15}N and CO under similar conditions. Complex **2**- ^{15}N has a lower energy stretch at 2137 cm^{-1} , consistent with metal bound isocyanate linkage.^{5h} Complex **2** was found to be paramagnetic based on a solution Evans magnetic susceptibility study ($\mu_{\text{eff}} = 2.53 \mu_{\text{B}}$, thf , 25 $^{\circ}\text{C}$), which is in accord with an $S = 1$ system of early first-row transition metals. Likewise, the ^1H NMR spectrum showed broad features over the range (13.90 to -2.79 ppm) at 25 $^{\circ}\text{C}$, again consistent with **2** being a paramagnet.

Given the poor yield of **2**, we turned our attention to a close relative of CO , the isocyanides CNR ($\text{R} = \text{'Bu}$ or $\text{Ad} = 1\text{-adamantyl}$). When **1** was treated with two equiv of CNR in DME , an immediate color change from orange to orange-brown or yellow-brown, resulted in the formation of reductively N–C coupled complexes $[\text{K}(\text{DME})_3][\text{(PN)}_2\text{Ti}(\text{NCNR})]$ ($\text{R} = \text{Ad}$; **3**; 'Bu , **4**) in moderate yields (**3**, 43%; **4**, 39%, Scheme 2). The formation of **3** and **4** was confirmed *via* a scXRD study and revealed the system to contain a cyanoamide ligand bound to a Ti^{II} -ate complex (middle, Figure 1).¹⁷ Akin to **2**, scXRD of **3** and **4**

Table 1. Salient metrical parameters^[a] and IR spectral data for the cumulene group in complexes divalent **2**–**5**, trivalent **6**–**8**, and tetravalent **9**. Distances are reported in \AA , angles in $^{\circ}$, and stretches in cm^{-1} .

Complex	2	3	4	5	6	7	8	9 ^[b]
$\text{Ti}-\text{N}_{\alpha}$	2.102(4)	2.092(3)	2.0857(16)	2.073(2)	1.9594(18)	1.9479(18)	1.9524(14)	1.998(4)
$\text{N}_{\alpha}-\text{C}$	1.170(6)	1.178(5)	1.195(3)	1.186(3)	1.227(3)	1.227(4)	1.209(2)	1.186(6)
$\text{C}-\text{O}/\text{N}_{\gamma}$	1.214(6)	1.282(5)	1.276(3)	1.258(3)	1.181(3)	1.228(4)	1.220(2)	1.234(6)
$\text{Ti}-\text{N}_{\alpha}-\text{C}$	172.3(4)	162.9(3)	167.40(16)	168.10(19)	170.66(19)	157.7(2)	167.15(13)	170.8(3)
$\text{N}_{\alpha}-\text{C}-\text{O}/\text{N}_{\gamma}$	179.7(6)	173.4(5)	173.8(2)	172.1(3)	178.3(3)	174.7(4)	171.08(19)	171.7(6)
$\nu(\text{NC})/(\text{N}^{15}\text{C})$	2196/2137	2192/2181	2118/2115	2172/2106	2207/2149	2121/2094	2143/2116	2255/2215

[a] Metrical parameters denotes bond metrics obtained from scXRD studies. [b] Although both NCNAd ligands in the *transoid* geometry of **9** are symmetrical, their bond metrics (distances in \AA , and angles in $^{\circ}$) slightly differ; $\text{Ti}-\text{N}_{\alpha}$, 2.001(4); $\text{N}_{\alpha}-\text{C}$, 1.192(6); $\text{C}-\text{N}_{\gamma}$, 1.248(7); $\text{Ti}-\text{N}_{\alpha}-\text{C}$, 167.5(4); $\text{N}_{\alpha}-\text{C}-\text{N}_{\gamma}$, 173.3(5).

RESEARCH ARTICLE

provided crucial structural information and highlighted rare examples of five-coordinate Ti^{II} complexes having trigonal bipyramidal geometries ($\tau_5 = 0.625$, **3**; $\tau_5 = 0.5977$, **4**). The structures also showed *transoid* phosphino groups ($\text{P}-\text{Ti}-\text{P}$: **3**, $170.72(4)^\circ$; **4**, $169.564(19)^\circ$) with a topologically linear TiNCNR linkage ($\text{Ti}-\text{N}-\text{C}$, $162.9(3)^\circ$ for **3** and $167.40(16)^\circ$ for **4**; $\text{N}-\text{C}-\text{N}$, $173.4(5)^\circ$ for **3** and $173.8(2)^\circ$ for **4**) resulting from C–N coupling of the isocyanides with the former titanium nitride ligand in **1**.^{14b} The $\text{Ti}-\text{N}$ distance for the carbodiimide ($2.092(3)$ Å, **3**; $2.0857(16)$ Å, **4**) is again quite long when compared to the much shorter $\text{Ti}\equiv\text{N}$ bond in **1** ($1.660(2)$ Å).^{14b} As a result, the TiNCN unit in **3** and **4** is nearly linear, most likely due to a significant degree of π -backbonding from the Ti^{II} ion into the π^* MO of the NCNR ligand, which inevitably causes the bond length in the CNR unit ($1.282(5)$ Å for **3**, and ($1.276(3)$ Å for **4**; Table 1) to be longer than that of free isocyanides.²⁰ Notably, the connectivity of **3** and **4** also reveals the K^+ being close to the $\gamma\text{-N}$, which tantalizingly implies a resonance more in accord with a Ti^{II} bound cyanoamide, $[\text{N}\equiv\text{C}-\text{NR}]^-$, ligand having a charge more formally localized on the $\gamma\text{-N}$, as opposed to $[\text{N}=\text{C}=\text{NR}]^-$.

Complexes **3** and **4** are paramagnetic, and a solution Evans magnetic susceptibility study reveals a $\mu_{\text{eff}} = 2.59 \mu_{\text{B}}$ ($g = 1.83$, **3**) and $2.42 \mu_{\text{B}}$ ($g = 1.71$, **4**) at 25°C , consistent with an $S = 1$ system, and their room temperature ^1H NMR spectrum shows broad features over a wide field range (14.24 to -16.72 ppm). Lastly, the IR spectra exhibit strong $\nu(\text{NC})$ stretches at 2192 and 2073 cm⁻¹ for **3** and 2118 and 2096 cm⁻¹ for **4**, which redshifted for their corresponding 50% ^{15}N isotopically enriched $[\text{K}(\text{DME})_3][(\text{PN})_2\text{Ti}^{(15)}\text{NCNR}]$ ($\text{R} = \text{Ad}$, **3- ^{15}N** ; $\text{R} = {^4\text{Bu}}$, **4- ^{15}N**) isotopomers.^{5c} These isotopomers are prepared from 50% ^{15}N enriched nitride **1- ^{15}N** and the corresponding isonitrile CNR.¹⁷ Regrettably and analogous to **2**, complexes **3** and **4** proved quite difficult to isolate in consistent yields given their reactive nature and also the presence of other impurities (vide infra). Therefore, we turned our attention to the more crystalline isonitrile substrate CNAd, as well as rendering the system into a discrete salt by encapsulation of the K^+ . Such an approach would also allow us to better understand the bonding and topology of the $\text{Ti}^{\text{II}}\text{NCNR}$ ligand due to any subtle distortions caused by electrostatic interactions and compare this to the discrete Ti^{II} cyanate salt **2**.

Following a similar protocol to **2**, treatment of **1** with CNAd in the presence of the cryptand, Kryptofix222 immediately resulted in precipitation of the discrete Ti^{II} salt $[\text{K}(\text{Kryptofix222})][(\text{PN})_2\text{Ti}(\text{NCNAd})]$ (**5**) in 49% yield (Scheme 2). Crystalline, dark brown **5** was also paramagnetic based on a solution Evans magnetic susceptibility study ($\mu_{\text{eff}} = 2.49 \mu_{\text{B}}$, thf, 25°C ; giving $g = 1.76$) and its ^1H NMR spectrum, which exhibits paramagnetically shifted resonances in the 16.02 to -1.15 ppm range. Similar to **3** and **4**, a strong $\nu(\text{NC})$ stretch was observed at 2172 and 2127 cm⁻¹, which redshifted to 2106 and 2071 cm⁻¹ for its 50% ^{15}N isotopically enriched isotopomer, $[\text{K}(\text{Kryptofix222})][(\text{PN})_2\text{Ti}^{(15)}\text{NCNAd}]$ (**5- ^{15}N**). Single crystals of **5** obtained from a concentrated thf solution at -35°C over 3 days allowed for a scXRD determination and confirmation of its connectivity. As shown in Figure 1, complex **5** is a discrete salt with no contacts between the encapsulated $\text{K}(\text{cryptand})^+$ component and the Ti^{II} fragment containing a $\text{Ti}^{\text{II}}\text{-cyanoamide}$ $[(\text{PN})_2\text{Ti}(\text{NCNAd})]^-$. The structure of **5** shows a five-coordinate Ti^{II} system with overall quite similar geometrical features to **3** and **4** as well as a linear TiNCNAd topology in accord with a cyanoamide $\text{Ti-N}\equiv\text{C-N-Ad}$ framework (Table 1). Despite complex **5** being formed in relatively better yields (49%), it was found again that other Ti species were produced in the mixture, thus precluding us from obtaining these Ti^{II} complexes (**2-5**) in pure form. It was speculated that any trace of Ti^{IV} (complex **1**) could be comproportionating with Ti^{II} species to form Ti^{III} .¹⁷ Consequently, we resorted to generating complexes **2-5** *in situ*, followed by immediate one-electron oxidation to what we speculated to be a more stable and neutral Ti^{III} species (vide infra). This strategy proved fruitful since the Ti^{III} cumulene species was not only more stable, but could be used as a precursor to improve the yield and purity of **2** and **5** *via* their one-electron reduction.

Construction and Structural Identification of Cumulene Motifs on Trivalent Titanium.

Given that complexes **2-5** are formed in relatively moderate yields, it was surmised that more stable forms of the cumulene species could be achieved *via* oxidation of the reaction mixture to convert the reactive Ti^{II} -ate species to corresponding neutral, less

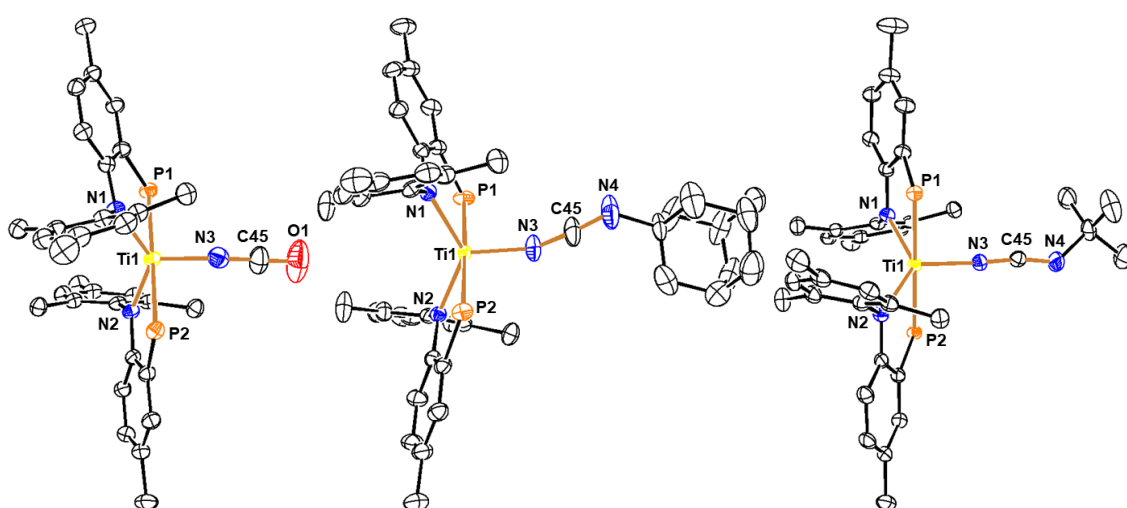


Figure 2. Molecular structures of the Ti^{III} complexes **6** (left), **7** (middle), and **8** (right) with thermal ellipsoids at the 50% probability level and hydrogen atoms are omitted for clarity.¹⁸

RESEARCH ARTICLE

reducing Ti^{III} derivative. Accordingly, adding CO (1 atm) or CNR (1 equiv) to nitride **1**, followed by the immediate addition of solid oxidant $[\text{Fc}][\text{OTf}]$ ($\text{Fc} = [\text{Fe}(\eta^5\text{-C}_5\text{H}_5)_2]^+$, 1 equiv) to the mixture, and immediate workup resulted in the isolation of the Ti^{III} species $[(\text{PN})_2\text{Ti}(\text{NCO})]$ (**6**) or $[(\text{PN})_2\text{Ti}(\text{NCNR})]$ ($\text{R} = \text{Ad}$, **7**; $\text{R} = ^\text{t}\text{Bu}$, **8**) in 89, 92, and 87 % yield, respectively (Scheme 2). An scXRD study of each confirmed the linear orientation of the isocyanate (N -bound) or carbodiimide ligand, with reduced π -backbonding between the Ti^{III} ion and the $\text{N}_\alpha\text{-C}$ moiety (Figure 2, Table 1) comprising the short C–O (in **6**) and C–N (in **7** and **8**) bond as compared to their corresponding Ti^{II} analogs. These findings are all in accord with the ligand being more representative of $\text{N}=\text{C}=\text{E}$ ($\text{E} = \text{O}$, NAd, and ^tBu) as opposed to $\text{N}\equiv\text{C}\text{-E}^-$. IR spectral data of **6–8**, as well as the respective ^{15}N enriched isotopomers $[(\text{PN})_2\text{Ti}^{(15)\text{NCO}}]$ (**6-¹⁵N**) and $[(\text{PN})_2\text{Ti}^{(15)\text{NCNR}}]$ ($\text{R} = \text{Ad}$, **7-¹⁵N**; $\text{R} = ^t\text{Bu}$, **8-¹⁵N**) also corroborate the presence of a strong $\nu(\text{CE})$ stretch, which redshifted for its respective ^{15}N enriched isotopologue (Table 1). Complexes **6–8** are paramagnetic having one-unpaired electron corroborated from solution state magnetic susceptibility study (Evans: $\mu_{\text{eff}} = 1.71(2)$ μ_{B} for **6**, 1.67(3) μ_{B} for **7**,

and **8-¹⁵N**) exhibited two 1e^- redox events centered at -2.42 V and -0.67 V vs. $\text{Fc}^{0/+}$ (0.00 V). Figure 3 shows a fully reversible cathodic wave at -2.42 V that is diffusion controlled, as implied by a Randles-Ševčík analysis (Figure 3b), which shows the linear correlation between i_p and $(V/s)^{1/2}$. Scanning anodically reveals a quasi-reversible anodic wave at -0.67 V when also judged on the Randles-Ševčík analysis (Figure S45), but this feature results in an additional peak forming at -1.63 V, thus clearly implying such a process to be irreversible under electrochemical conditions. The quasi-reversible wave at -0.67 V suggested that one-electron chemical oxidation of **7** could result in formation of a putative $[(\text{PN})_2\text{Ti}^{\text{IV}}(\text{NCNAd})]^+$ at the electrode surface, but that such a species is unstable under electrochemical conditions. Further studies confirmed that the chemical oxidation of **7** does indeed result in the formation of a new species, which we were able to identify and characterize (vide infra).

Keeping an eye on the reactive nature of Ti^{II} cumulene species from a nitride anion precursor, we suspected that generating the electride from KC_8 and the cryptand would facilitate the reduction of Ti^{III} cumulenes and facile separation of the pure salt.²¹ To our delight, chemical reduction of **6** and **7** with KC_8 in the presence of Kryptofix222 in toluene over a period of 3 h resulted in clean formation of the Ti^{II} salt species **2** and **5** in 92% and 94% yields, respectively (Scheme 2). This route allowed us to obtain divalent complexes in bulk and pure form to probe them spectroscopically. Complexes **2** and **5** still are metastable and decompose gradually over 8 days, even when stored as solids at -35 °C.

EPR Spectroscopic Studies of Divalent and Trivalent Complexes. Although the reductively coupled ate complexes **3** and **4** are readily decomposed even when stored as solids at low temperatures, complexes **2** and **5** are metastable and amenable to further spectroscopic studies. Since these are d^2 (non-Kramers) species, we resorted to employ high-frequency and -field electron paramagnetic resonance (HFEPR) spectroscopy.²²

Both complexes **2** and **5** measured as solids at cryogenic temperatures yielded HFEPR spectra of outstanding quality and easily interpretable as originating from the triplet ($S = 1$) spin state. Figures 4 and S47–S50 show their representative spectra accompanied by simulations assuming a powder distribution of microcrystallites and using the standard spin Hamiltonian shown in equation 1. The parameters included in Table 2 were obtained through the tunable-frequency methodology (see Figure S50), containing the previously reported complex $[(\text{K}(\text{Kryptofix222}))(\text{PN})_2\text{TiCl}]$.²³

$$\hat{H} = \mu_B \mathbf{B} \{ \mathbf{g} \} \hat{\mathbf{S}} + D \left\{ \hat{S}_z^2 - \frac{1}{3} S(S+1) \right\} + E (\hat{S}_x^2 - \hat{S}_y^2) \quad (\text{eq. 1})$$

A detailed analysis of these spin Hamiltonian parameters is beyond the scope of this reactivity oriented study, but we note qualitatively that although the three Ti^{II} complexes listed in Table 2 are very similar, the strongest ligand, in terms of both σ -donation and π -acceptance, carbodiimide, (in **5**) has the smallest D value

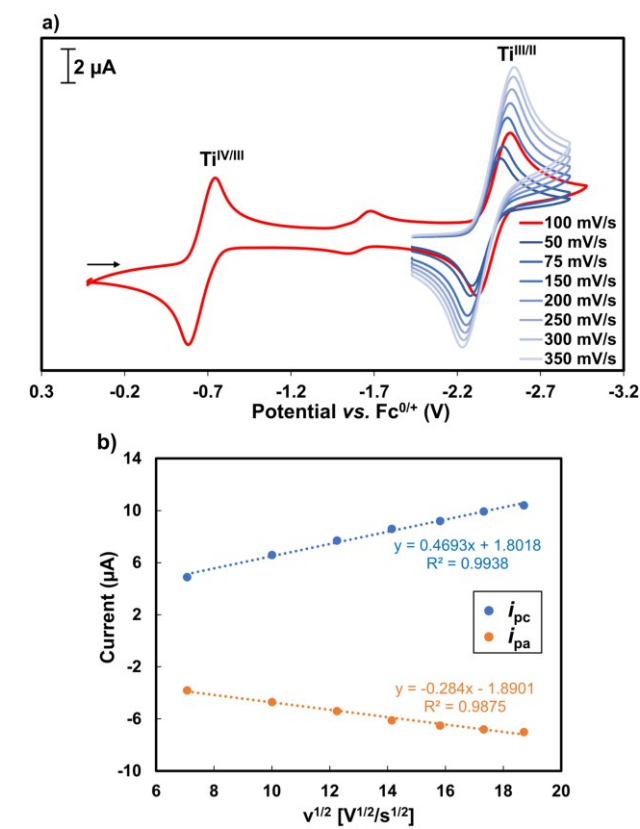


Figure 3. a) Cyclic voltammograms (CVs) of **7** in THF with 0.1 M $[^t\text{Bu}_4\text{N}][\text{PF}_6]$. Full range CV with 0.1 V/s scan rate (red trace); blue traces are CVs of only the reversible redox event of the $\text{Ti}^{\text{III/IV}}$ couple with various scan rates as indicated. b) Randles-Ševčík plot for redox event of the $\text{Ti}^{\text{III/IV}}$ couple.

1.85(2) μ_{B} for **8**; C_6D_6 , 25 °C).

To gain further insight into the redox chemistry of the trivalent titanium, we collected a cyclic voltammogram (CV) of the model compound **7**. The squarewave voltammetry of **7** in THF with 0.1 M electrolyte $[^t\text{Bu}_4\text{N}][\text{PF}_6]$ (Figure 3a, S43

Table 2. Spin Hamiltonian parameters for $[(\text{PN})_2\text{Ti}^{\text{II}}(\text{X})]^-$.

Complex	X ⁻	g_x	g_y	g_z	D , cm ⁻¹	E , cm ⁻¹	E/D
ref ²³	Cl	1.960	1.953	1.995	+2.137	+0.081	0.038
2	NCO	1.966(1)	1.959(1)	1.998(2)	+1.967(5)	+0.063(2)	0.032
5	NCNAd	1.969(1)	1.965(1)	2.000(1)	+1.845(2)	+0.059(1)	0.032

RESEARCH ARTICLE

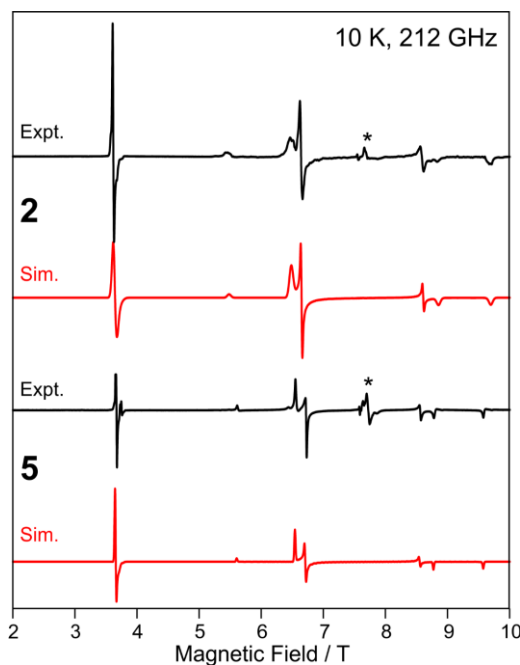


Figure 4. HFEPR spectra of powdered samples of **2** (top) and **5** (bottom), recorded at 10 K with microwave frequency 212.000 GHz (black traces). Red traces are simulations for $S = 1$ with parameters as in Table 2. The two features appearing at ~ 7.7 T (asterisks) in each complex are due to a minute amount of Ti^{III} impurity ($g \sim 1.96$) and an unidentified radical ($g \sim 2.00$), not simulated.

while the weakest donor, chloride,²³ has the largest. Note that the d_{x^2}, d_{y^2} orbitals are coupled by \hat{l}_x, \hat{l}_y to $d_{xy}, d_{x^2-y^2}$ providing a mechanism for zero-field splitting (zfs) in the $S = 1$ Ti^{II} congeners. Qualitatively, stronger ligands would increase the relative energy of electronic excited states with populated σ anti-bonding orbitals ($d_{xy}, d_{x^2-y^2}$) relative to the ground state (d_{x^2}, d_{y^2} ; *vide infra*) with populated π -backbonding orbitals, which reduces their contribution to zfs. The greater separation between these two sets of orbitals in **5** vs. **2** vs. the chlorido complex may thus be the basis for the corresponding decrease in D (Table 2).

Given that complexes **6–8** contain one unpaired electron (*vide supra*), we collected their CW X-band EPR spectra (Figure 5). The room temperature (293 K) spectrum of a 1.0 mM toluene solution of **6** showed an isotropic signal with an effective g -value $g_{\text{iso}} = 1.97$, which splits into a 3-line pattern in a 1:2:1 ratio due to hyperfine (hf) coupling to both P nuclei (^{31}P , $I = 1/2$, 100% natural abundance) and was determined as $A_{\text{iso}} = 18.8 \times 10^{-4} \text{ cm}^{-1}$ (2.0 mT) (Figure S51). As shown in the top left panel of Figure 5, upon decreasing the modulation amplitude from 1.0 to 0.1 mT, further hf coupling, $A_{\text{iso}} = 2.20 \times 10^{-4} \text{ cm}^{-1}$ (0.2 mT), involving the two symmetry equivalent N nuclei could also be resolved (^{14}N , $I = 1$, 99.6% natural abundance). At 95 K, in frozen solution, the spectrum changes into an axial signal with hf coupling to both P nuclei, which was detected at both g -values ($g_{\parallel} = 1.99$, and $g_{\perp} = 1.97$) as $A_{\parallel} = 20.1 \times 10^{-4} \text{ cm}^{-1}$ (2.2 mT), and $A_{\perp} = 20.3 \times 10^{-4} \text{ cm}^{-1}$ (2.2 mT) (top right, Figure 5). This supports the high symmetry of **6** due to the linear cumulene moiety. In contrast, the room temperature (293 K) solution spectrum of a 1.0 mM toluene solution of **7** features axial symmetry with effective g -values $g_{\parallel} = 1.98$, $g_{\perp} = 1.95$, and hf coupling to both ^{31}P nuclei as $A_{\parallel} = 20.0 \times 10^{-4} \text{ cm}^{-1}$ (2.2 mT), and $A_{\perp} = 19.6 \times 10^{-4} \text{ cm}^{-1}$ (2.2 mT) (middle left, Figure 5). However, the frozen toluene CW

X-band EPR spectrum of **7** at 95 K shows rhombic symmetry ($g_1 = 1.98$, $g_2 = 1.96$, $g_3 = 1.90$), with resolved hf coupling to two ^{31}P nuclei as $A_1 = 19.0 \times 10^{-4} \text{ cm}^{-1}$ (2.1 mT), and $A_2 = 18.3 \times 10^{-4} \text{ cm}^{-1}$ (2.0 mT) (middle right, Figure 5). To conclusively determine if hf coupling was due to the carbodiimide N, we also collected CW X-band EPR spectra on the 50% ^{15}N enriched isotopomer **7-¹⁵N**, but found the spectra to have identical features to natural abundance **7** (blue trace, middle spectra in Figure 5). Therefore, while the unpaired electron is likely based in a metal centric orbital, the hyperfine coupling solely derives from the chelating PN phosphorus and nitrogen nuclei and not the former nitride nitrogen atom. The CW X-band EPR spectrum of **8** showed similar features to that of complex **7**, but with some subtle differences such as rhombic symmetry at 293 K with effective anisotropic g -values ($g_1 = 1.98$, $g_2 = 1.96$, and $g_3 = 1.95$) having hf coupling to two ^{31}P nuclei as $A_1 = 19.3 \times 10^{-4} \text{ cm}^{-1}$ (2.1 mT), $A_2 = 18.9 \times 10^{-4} \text{ cm}^{-1}$ (2.1 mT), and $A_3 = 20.9 \times 10^{-4} \text{ cm}^{-1}$ (2.3 mT) (bottom left,

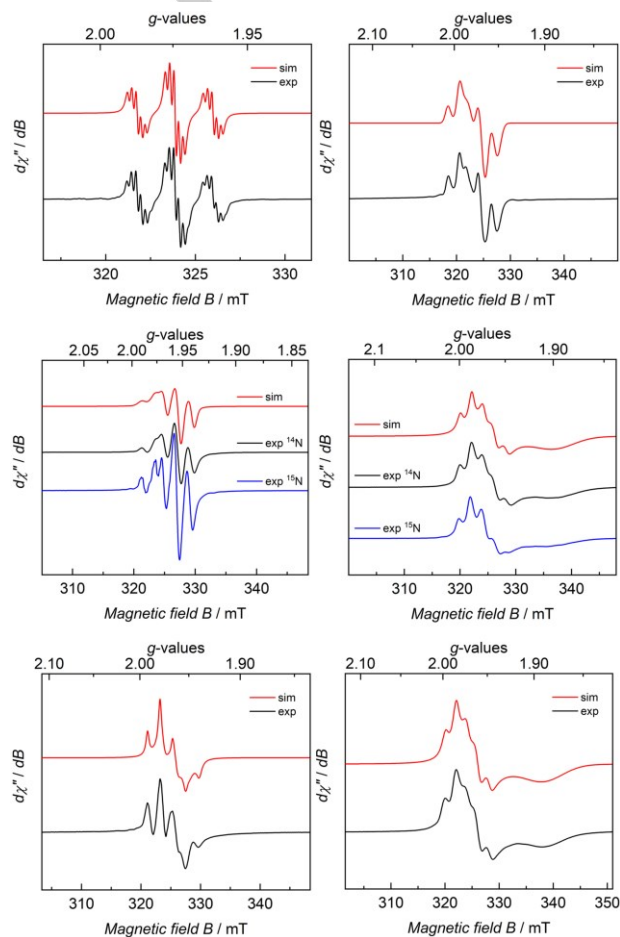


Figure 5. Top: CW X-band EPR spectrum of **6** (black trace) recorded as a 1 mM solution in toluene at 293 K (left) and 95 K (right) and its simulation (red trace). Experimental conditions left: microwave frequency (ν) = 8.939 GHz, modulation amplitude (MdA) = 0.1 (left) and 0.5 mT (right), microwave power (MP) = 1.0 mW, modulation frequency (MdF) = 100 kHz, time constant (tc) = 0.1 s. Middle: CW X-band EPR spectra for **7** (black trace) and isotopically enriched **7-¹⁵N** (blue trace) recorded as a 1 mM solution in toluene at 293 K (left) and 95 K (right) and its simulation (red trace). Experimental conditions: microwave frequency ν = 8.959 GHz, MdA = 1.0 (^{14}N) and 0.3 (^{15}N) mT (left) and 0.1 mT (right), MP = 1.0 mW, MdF = 100 kHz, tc = 0.1 s. Bottom: CW X-band EPR spectrum of **8** (black trace) recorded as a 1 mM solution in toluene at 293 K (left) and 95 K (right) and its simulation (red trace). Experimental conditions: ν = 8.944 GHz, MdA = 1.0 (left) and 0.1 (right) mT, MP = 1.0 mW, MdF = 100 kHz, tc = 0.1 s. Simulation parameters for all spectra are reported in the SI.

RESEARCH ARTICLE

Figure 5). Moreover, at low temperature, in frozen toluene solution (95 K), the CW X-band EPR spectrum evolves into a rhombic signal with hf coupling to both ^{31}P nuclei, which was further resolved at two of the three g values and was determined to be $A_1 = 18.5 \times 10^{-4} \text{ cm}^{-1}$ (2.0 mT), and $A_2 = 18.8 \times 10^{-4} \text{ cm}^{-1}$ (2.1 mT) (bottom right, Figure 5). Notably, the EPR spectrum at liquid helium temperature (7–9 K) did not lead to any additional spectral improvement (Figure S56). Thus, the EPR spectral signatures for **6–8** are consistent with the unpaired electron being housed in a metal centric orbital, which is relatively non-bonding (d_{x^2} and/or d_{yz}) and might be perpendicular to the cumulene moiety assuming the trigonal bipyramidal geometry in these systems.

Structural Identification of the Carbodiimide Motif on Tetravalent Titanium. To chemically access a tetravalent and putative species such as $[(\text{PN})_2\text{Ti}(\text{NCE})]^+$ from a Ti^{III} precursor, we turned to a weak oxidant (e.g., the oxidation potential of **7** was -0.67 V when judged by its CV data, *vide supra*), but also one having a weakly coordinating anion to minimize disruption of the cumulene moiety and preserve the same coordination number on Ti^{IV} . Attempts at chemical oxidation of **6** resulted in a myriad of products that were not further pursued; however, treatment of **7** with $[\text{Fc}^*][\text{B}(\text{C}_6\text{F}_5)_4]$ ^{24a,24b} ($\text{Fc}^* = [\text{Fe}(\text{C}_5\text{Me}_5)_2]^+$)^{24c} yielded an immediate color change from red to blood red. Workup of the reaction mixture in *thf* allowed isolation of the *bis*-carbodiimide Ti^{IV} complex $[(\text{PN})_2\text{Ti}(\text{NCNAd})_2]$ (**9**) in 34% yield (Figure 6a). The reaction mixture did contain other intractable materials, most likely originating from ligand disproportionation and decomposition of what we propose to be putative dication $[(\text{PN})_2\text{Ti}(\text{thf})_2]^{2+}$. Once isolated, NMR spectral data revealed complex **9** to possess C_s symmetry evident from symmetrical ^1H NMR spectral features along with an equivalent phosphorus environment (^{31}P NMR: 34.0 ppm).¹⁷ The scXRD confirmed the

carbodiimide groups to be *transoid*, whereas the phosphino and anilido nitrogens for the PN ligands are *cisoid* to each other (Figure 6b). Metrical parameters for the two NCNAd scaffolds do not deviate significantly from its predecessor **7**, but the Ti–N bonds are slightly elongated most likely due to *trans*-influence (Table 1). Preparing the 50% ^{15}N enriched isotopomer $[(\text{PN})_2\text{Ti}(\text{N}^{15}\text{C}^{15}\text{NAd})_2]$ (**9-¹⁵N**) showed a single resonance at 60.0 ppm in the ^{15}N NMR spectrum,^{10m} whereas the IR spectrum further demonstrated a red shifted $\nu(\text{NC})$ at 2215 cm^{-1} , when compared to unlabeled **9** ($\nu(\text{NC})$ at 2253 cm^{-1}).²⁵ These high energy stretches are consistent with essentially little or no π -backbonding taking place (Table 1).^{5f}

Computational Studies and Understanding of Bonding and Structure of the NCE (E = O or NAd) Fragment in Ti^{II} , Ti^{III} , and Ti^{IV} Ions. To shed light on the bonding characteristics, especially the extent of electron delocalization along the Ti–NCE functionality with Ti^{II} , Ti^{III} , and Ti^{IV} centers, we turned to density functional theory (DFT) calculations (see SI for details).¹⁷

Our simulations on non-truncated molecular models revealed equilibrium structures for $[(\text{PN})_2\text{Ti}^{\text{II}}(\text{NCO})]^-$ (anion of **2**), $[(\text{PN})_2\text{Ti}^{\text{III}}(\text{NCNAd})]^-$ (anion of **5**), $(\text{PN})_2\text{Ti}^{\text{III}}(\text{NCO})$ (**6**),

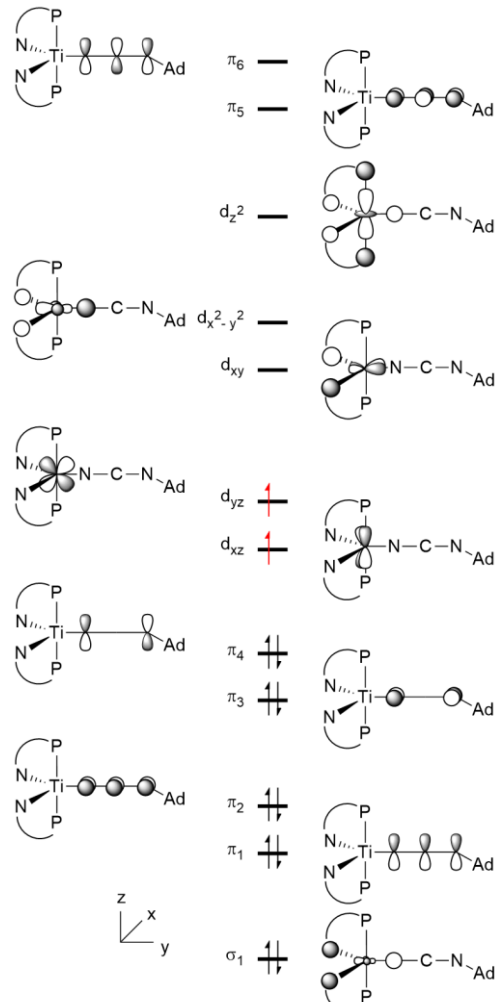


Figure 7. Formal description of the electronic structure for the NCNAd ligand in the anionic component of complex **5** and interactions with the Ti^{II} ion within molecular orbital theory, assuming an effective trigonal-bipyramidal geometry around the metal. SOMO's are shown with red-colored electrons.

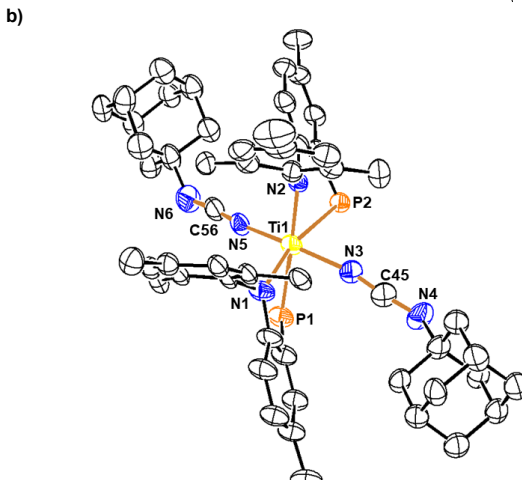
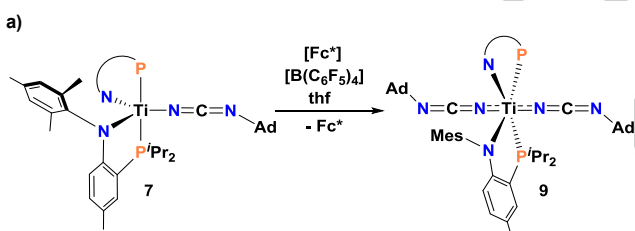


Figure 6. a) Oxidation of **7** with $[\text{Fc}^*][\text{B}(\text{C}_6\text{F}_5)_4]$ to form **9**. b) Molecular structures of the Ti^{IV} complex **9** with thermal ellipsoids at the 50% probability level. Residual solvent molecules and hydrogen atoms are omitted for clarity.¹⁸

RESEARCH ARTICLE

(PN)₂Ti^{III}(NCNAd) (**7**), and (PN)₂Ti^{IV}(NCNAd)₂ (**9**), that are in excellent agreement with the experimentally observed geometries obtained from scXRD (Tables S7 – S11). In agreement with the above described measurements, solution-state DFT also predicts reduction potentials of –2.58 V and –0.89 V vs. Fc^{0/+} for the Ti^{III}/Ti^{II} and Ti^{IV}/Ti^{III} redox couples of the terminal Ti carbodiimide **7**, respectively. Also, in agreement with CW X-band EPR spectroscopy, computational studies predict a doublet ground state for the neutral Ti^{III} species **7**, featuring a non-bonding metal-centered radical having δ symmetry to the –NCNR moiety (d_{xz} , SOMO in Figure 8). These benchmarks convincingly substantiate our methodology, i.e., the computed structures capture salient characteristics of these molecular systems, including their electronic structures.

We used quasi-restricted orbitals (QROs), molecular orbital composition analyses, Mayer bond orders, and atomic charges to analyze and characterize the nature of bonding of the Ti–NCO and NCNAd functionalities in the Ti^{II} anionic fragments of **2** and **5**, Ti^{III} neutral species **6** and **7** and the hypothetical Ti^{IV} cationic complexes $[(PN)_2Ti^{IV}(NCO)]^+$ (**10**) and $[(PN)_2Ti^{IV}(NCNAd)]^+$ (**11**), i.e., the likely intermediates from the one-electron oxidized forms of **6** and **7**, respectively. Figure 7 formally describes the electronic structure along the NCNAd ligand in **5** and predicts two perpendicular sets of –NCNR π orbitals, i.e., π_1 – π_4 – π_6 and π_2 – π_3 – π_5 , each corresponding to the classical three-center three-atomic-orbital system: a full in-phase bonding combination (π_1 and π_2), one with a nodal plane across the central carbon atom (π_3 and π_4), and finally the antibonding combination (π_5 and π_6). While π_1 and π_2 represent two π bonds along the N–C–N axis, π_3 and π_4 characterize lone pairs at the terminal atoms. Two d-orbitals have π symmetry; the formally non-bonding d_{yz} and d_{xy} of high energy due to being antibonding with two equatorial ligand donor orbitals in the σ subspace. The d_{xz} orbital is also non-bonding and of lower energy, but more notably, this orbital has δ symmetry to the –

NCNR fragment and, thus, does not overlap. In this arrangement, the mixing of π_3 with d_{xy} and π_4 with d_{yz} represents ligand to metal π donation, whereas the combination of d_{yz} , if filled or semi-filled, with π_6 is characteristic of metal to ligand π back-donation (Figure 7).

The quasi-restricted molecular orbitals (Figures S64–S69) computed for Ti^{II} fragments of **2**, **5**; Ti^{III} complexes **6**, **7** (Figure 8), and hypothetical Ti^{IV} fragments **10**, **11**, align perfectly with this formal description. The atomic composition of the orbitals implies that π -backdonation is negligible in **5** (Ti^{II}) and nonexistent in both **7** (Ti^{III}) and **11** (Ti^{IV}), as the π -backdonating d_{yz} is unoccupied in the latter two species. Noteworthy, the energy mismatch between d_{xy} and π_3 is so large in all species that their mixing is negligible. This notion can be witnessed in HOMO-10 of **7** (Figure 8), with only a 2.2% Ti contribution in the ligand π_3 orbital. Thus, the key differences in the Ti–NCNAd bonding topology for Ti^{II}, Ti^{III}, and Ti^{IV} originate solely from the π donation from π_4 to d_{yz} , which increases gradually when going from the Ti^{II} fragment of **5** to Ti^{III} (**7**) and Ti^{IV} (**11**). This π donation is portrayed unmistakably by the HOMO-4 of **7** in Figure 8, with a 14% relative contribution from Ti to the total orbital composition of the Ti–NCNAd scaffold (relative contribution is calculated from the total contributions of atoms to an MO localized on the Ti–NCE fragment, i.e., %Ti / (%Ti + %N_α + %C + %N_γ)). The analogous orbitals have a relative Ti contribution of 4% and 18% in **5** and **11**, respectively, thus demonstrating an increasing π donation as the oxidation state increases. The same conclusions can be drawn from the terminal Ti–NCO functionalities in **2**, **6** and the hypothetical cation fragment of **10** (Figures S64–S66), having the relative increasing Ti contribution in HOMO-11: Ti^{II} (2%) < Ti^{III} (8%) < Ti^{IV} (11%) (Figure 8).

As shown in Figure 8, and in agreement with the CW X-band EPR spectroscopic measurements for the Ti^{III} species **6**–**8**, the unpaired electron is housed in a non-bonding and metal-centered orbital of δ symmetry that is perpendicular to the cumulene moiety (d_{xz} in Figure 7 and SOMO in Figure 8). Hence, no interaction of the unpaired electron is possible with the cumulene in accordance with the EPR-spectra showing similar features for **7** and its isotopomer **7**–¹⁵N (vide supra, middle spectra of Figure 5). Figure 8 also reveals the topologies of HOMO-4 in Ti^{III}, which suggest some π donation from the –NCNAd fragment to the Ti^{III} core, which accounts for the experimentally observed decrease in the Ti–N_α distance (1.95 vs. 2.07 Å) and an increase in the Ti–N_α bond order (0.80 vs. 0.54) with respect to the Ti^{II} fragment in **5** (vide supra). The depopulation of the d_{yz} orbital (Figures 7 and 8) when going from Ti^{II} to Ti^{III} may also diminish the repulsion along the Ti–N_α and C–N_γ axes, leading to the observed strengthening of the Ti–N_α and C–N_γ bonds (Figure 9). Admittedly, a decrease in the attraction between the N_α–C bond also occurs, manifested in the slight elongation of such bond. We observed the same structural

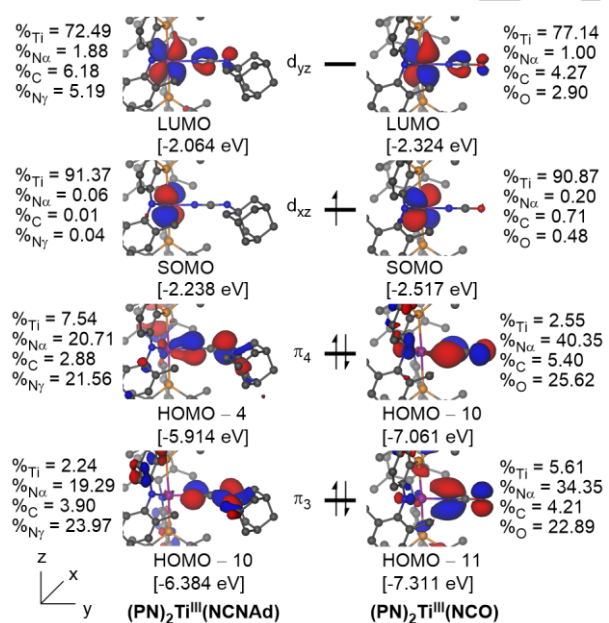


Figure 8. Relevant QROs of the neutral Ti^{III} complexes **6** (right) and **7** (left) characterizing the increasing π -donation from the metal center to the π -system of the –NCNR–NCO fragment. Mulliken orbital compositions for the Ti, and cumulene atoms are also listed. %s display the total contribution of an atom to the molecular orbital. Hydrogen atoms are omitted for clarity.

RESEARCH ARTICLE

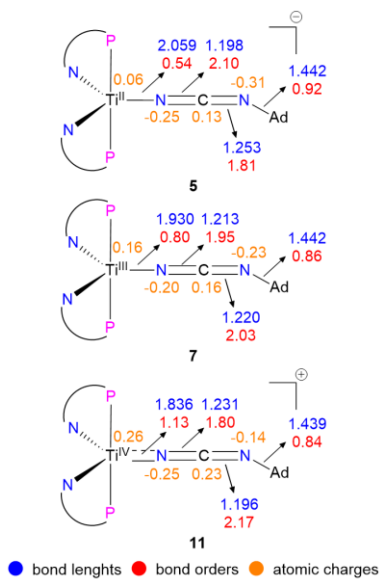
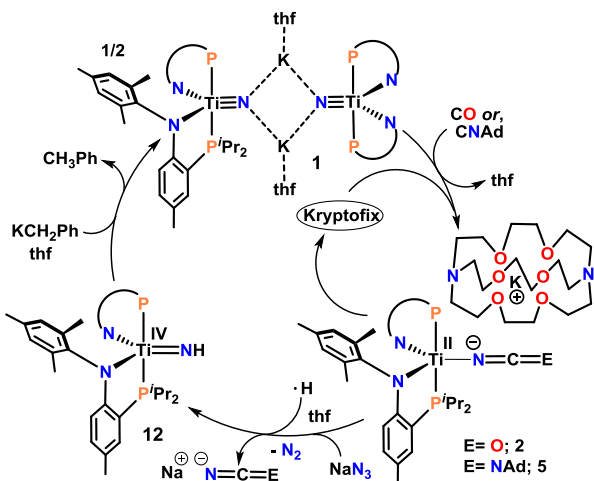


Figure 9. Bond lengths, Mayer bond orders and dipole moment corrected Hirschfeld atomic charges of anionic Ti^{II} fragment of **5**, the neutral Ti^{III} complex **7** and the hypothetical cationic Ti^{IV} fragment **11**.

changes and trends (Figure S63) for the corresponding analogs **2** (anion fragment), **6**, and **10** (cation fragment).

This molecular orbital analysis establishes that the electronic structure of the cumulene species **5**, **7**, and **11** can be best represented by a dominant $\text{Ti}-\text{N}_\alpha=\text{C}=\text{N}-\text{R}$ Lewis resonance structure, with a non-negligible contribution from the $\text{Ti}=\text{N}=\text{C}=\text{N}-\text{R}$ form only in the case of Ti^{IV} , i.e., **11**. This conclusion conforms to the bond order indices, atomic charges and bond lengths summarized in Figure 9. Namely, $\text{N}=\text{C}$ bond orders fluctuate between 1.8 and 2.2 in all species, and the charge distribution along $\text{N}=\text{C}=\text{N}-\text{R}$ remains alike for **5**, **7**, and **11**. On the other hand, there is a sharp increase in the $\text{Ti}-\text{N}_\alpha$ bond order and shortens of this bond as going from Ti^{II} to Ti^{III} and Ti^{IV} . This results attributed from π donation of the $-\text{NCNR}$ fragment to the metal, which can be expressed by mixing of $\text{Ti}=\text{N}=\text{C}=\text{N}-\text{R}$ into the dominant $\text{Ti}-\text{N}_\alpha=\text{C}=\text{N}-\text{R}$ resonance form.

A Cycle for N-Atom Transfer to π -Acids Using Complex **1, NaN_3 and a Base.** The fact that CO and isocyanides such as CNAd and CN⁺Bu readily coupled with the nitride ligand in **1** to form a Ti^{II} ion having a dative cumulene salt tantalizingly suggested that such a process could be rendered catalytic in the presence of excess N_3^- and π -acid. Cummins^{5a} and Kawaguchi^{5c} have used a V^{III} trisanilide and V^{III} N-(*p*-tolyl)-4-^tBu-anilido-2,6-bis-aryloxido systems respectively, to promote N-atom transfer to CO, whereas, Smith^{5f} used tris(carbene)borate based Fe^{IV} -nitride and Bertrand²⁶ used bis(imidazolidin-2-iminato)phosphononitrile for N-atom transfer to isocyanides. Meyer and co-workers have also documented a cycle for N-atom transfer using a U^{III} complex, N_3SiMe_3 (N-atom source), CNCH_3 , CH_2Cl_2 and a reductant.²⁷ Although treatment of **1** with CO and CNAd in the presence of cryptand and NaN_3 in *thf* resulted in immediate formation of parent cumulene salts such as NaNCO and NaNCNAd , respectively (confirmed by IR spectroscopy),¹⁷ catalysis was shunned due to the deleterious formation of the parent imide $[(\text{PN})_2\text{Ti}(\text{NH})]$ via an unstable and putative Ti^{II} azide intermediate



Scheme 3. A synthetic cycle for N-atom transfer from **1** to CO and CNAd using NaN_3 and a strong base such as KCH_2Ph with concomitant formation of NaNCE ($\text{E} = \text{O}$ or, NAd).

$[\text{K}(\text{Kryptofix}222)][(\text{PN})_2\text{Ti}(\text{N}_3)]$. Previous studies have invoked the extrusion of N_2 from $[(\text{PN})_2\text{Ti}(\text{N}_3)]$ to accompany the formation of a transient nitridyl radical $[(\text{PN})_2\text{Ti}(\text{N}\cdot)]$, which engages in H-atom abstraction, most likely from the PN ligand.²⁸ As a result, a catalytic cycle involving N-atom transfer from **1** to CO and CNAd is not yet possible due to the inaccessibility of direct formation of titanium nitride anion complex, **1**, rather the detrimental parent imide, **12** is formed (Scheme 3). Despite the parent imido forming from this reaction, we could close the synthetic cycle for N-atom transfer by treating $[(\text{PN})_2\text{Ti}(\text{NH})]$ with KCH_2Ph to reform the nitride moiety as shown in Scheme 3.

Conclusion

In summary, we demonstrate how a nucleophilic titanium nitride reacts with carbon monoxide or alkyl isocyanides *via* two electron reductive N-C coupling to prepare rare examples of five-coordinate Ti^{II} cumulene complexes. Having a low-valent system provided the opportunity to probe how the assembled cyanate and amidonitrile moiety changes into their corresponding isocyanate and carbodiimide motif, upon changing of the metal oxidation state from $\text{Ti}^{\text{II}} \rightarrow \text{Ti}^{\text{III}}$ and vice versa. Thus, the $\text{Ti}-\text{N}$ distances and the topology of the NCN motif were somewhat sensitive to changes in the titanium oxidation state. This feature is likely attributed to the unpaired electrons (e.g., d^2 and d^1 systems) being mostly metal centric and $e^- - e^-$ repulsions being more critical in the $\text{Ti}-\text{N}$ bonding. Moreover, 1e^- oxidation of Ti^{III} resulted in the formation of Ti^{IV} , which benefits from greater π -donation, in accord with decreasing repulsions as the d-electron count decreases: $\text{Ti}^{\text{II}} \rightarrow \text{Ti}^{\text{III}} \rightarrow \text{Ti}^{\text{IV}}$. Our study also demonstrates that maximum covalency is present in a neutral Ti^{III} cumulene moiety. We also show a synthetic cycle for N-atom transfer *via* reductive N-C coupling using a titanium nitride, which provides a unique opportunity for the formation of cyanate and carbodiimide salts and their isotopically labelled products.

Acknowledgments

RESEARCH ARTICLE

We thank the University of Pennsylvania and the Chemical Sciences, Geosciences, and Biosciences Division, Office of Basic Energy Sciences, Office of Science, U.S. DOE (DEFG02-07ER15893 to D.J.M.). We thank Drs. Patrick J. Carroll, Brian Manor, and Taylor M. Keller for their help in solving certain crystal structures. B.P. thanks UTEP for a Rising STARS grant (E210291776). The authors thank UTEP HPC JAKAR Cluster for the computational resources provided free of charge. K.M. and D.F. thank the Friedrich-Alexander-Universität Erlangen-Nürnberg (FAU) for generous financial support. Part of this work was performed in the National High Magnetic Laboratory, funded by the NSF (Cooperative Agreement DMR-2128556) and the State of Florida.

Conflict of Interest

The authors declare no conflict of interest.

Keywords: nitride, atom transfer, reductive coupling, structural interpretation, reactivity, titanium

[1] a) S. D. Roughley, A. M. Jordan, *J. Med. Chem.* **2011**, *54*, 3451–3479; b) Padwa, A. in *Comprehensive Heterocyclic Chemistry III* (eds A. R. Katritzky, C. A. Ramsden, E. F. V. Scriven, R. J. K. Taylor) 1–104 (Elsevier, 2008); c) Aziridines and Epoxides in Organic Synthesis (Ed.: A. K. Yudin), Wiley-VCH, Weinheim, **2006**; d) P. Q. Kelly, A. S. Filatov, M. D. Levin, *Angew. Chem. Int. Ed.* **2022**, *61*, e202213041; *Angew. Chem.* **2022**, *134*, e202213041; e) A. J. Keane, W. S. Farrell, B. L. Yonke, P. Y. Zavalij, L. R. Sita, *Angew. Chem. Int. Ed.* **2015**, *54*, 10220–10224; *Angew. Chem.* **2015**, *127*, 10358–10362; f) M. N. Cosio, D. C. Powers, *Nat Rev Chem* **2023**, *7*, 424–438; g) T. Itabashi, K. Arashiba, A. Egi, H. Tanaka, K. Sugiyama, S. Suginome, S. Kuriyama, K. Yoshizawa, Y. Nishibayashi, *Nat. Commun.* **2022**, *13*, 6161.

[2] a) W.-L. Man, W. W. Y. Lam, S.-M. Yiu, T.-C. Lau, S.-M. Peng, *J. Am. Chem. Soc.* **2004**, *126*, 15336–15337; b) D. W. Crandell, S. B. Muñoz, J. M. Smith, M.-H. Baik, *Chem. Sci.* **2018**, *9*, 8542–8552; c) S. B. Muñoz, W. Lee, D. A. Dickie, J. J. Scepaniak, D. Subedi, M. Pink, M. D. Johnson, J. M. Smith, *Angew. Chem. Int. Ed.* **2015**, *54*, 10600–10603; *Angew. Chem.* **2015**, *127*, 10746–10749; d) J. M. Smith, in *Progress in Inorganic Chemistry* (Ed.: K.D. Karlin), Wiley, **2014**, pp. 417–470; e) W.-L. Man, W. W. Y. Lam, T.-C. Lau, *Acc. Chem. Res.* **2014**, *47*, 427–439.

[3] a) A. G. Maestri, K. S. Cherry, J. J. Toboni, S. N. Brown, *J. Am. Chem. Soc.* **2001**, *123*, 7459–7460; b) W.-T. Lee, R. A. Juarez, J. J. Scepaniak, S. B. Muñoz, D. A. Dickie, H. Wang, J. M. Smith, *Inorg. Chem.* **2014**, *53*, 8425–8430.

[4] a) C. Leung, T. Wong, T. Lau, W. Wong, *Eur J Inorg Chem* **2005**, *2005*, 773–778; b) C. Besson, J.-H. Mirebeau, S. Renaudineau, S. Roland, S. Blanchard, H. Vezin, C. Courillon, A. Proust, *Inorg. Chem.* **2011**, *50*, 2501–2506.

[5] a) J. S. Silvia, C. C. Cummins, *J. Am. Chem. Soc.* **2009**, *131*, 446–447; b) L. Tran, M. Pink, X. Gao, H. Park, D. J. Mindiola, *J. Am. Chem. Soc.* **2010**, *132*, 1458–1459; c) Y. Ishida, H. Kawaguchi, *J. Am. Chem. Soc.* **2014**, *136*, 16990–16993; d) J. A. Buss, C. Cheng, T. Agapie, *Angew. Chem. Int. Ed.* **2018**, *57*, 9670–9674; *Angew. Chem.* **2018**, *130*, 9818–9822; e) S. D. Brown, M. P. Mehn, J. C. Peters, *J. Am. Chem. Soc.* **2005**, *127*, 13146–13147; f) J. J. Scepaniak, R. P. Bontchev, D. L. Johnson, J. M. Smith, *Angew. Chem. Int. Ed.* **2011**, *50*, 6630–6633; *Angew. Chem.* **2011**, *123*, 6760–6763; g) B. Askevold, J. T. Nieto, S. Tussupbayev, M. Diefenbach, E. Herdtweck, M. C. Holthausen, S. Schneider, *Nat. Chem.* **2011**, *3*, 532–537; h) P. A. Cleaves, D. M. King, C. E. Kefalidis, L. Maron, F. Tuna, E. J. L. McInnes, J. McMaster, W. Lewis, A. J. Blake, S. T. Liddle, *Angew. Chem. Int. Ed.* **2014**, *53*, 10412–10415; *Angew. Chem.* **2014**, *126*, 10580–10583; i) M. Falcone, L. Chatelain, R. Scopelliti, I. Živković, M. Mazzanti, *Nature* **2017**, *547*, 332–335; j) M. Falcone, C. E. Kefalidis, R. Scopelliti, L. Maron, M. Mazzanti, *Angew. Chem. Int. Ed.* **2016**, *55*, 12290–12294; *Angew. Chem.* **2016**, *128*, 12478–12482.

[6] a) H.-K. Kwong, W.-L. Man, J. Xiang, W.-T. Wong, T.-C. Lau, *Inorg. Chem.* **2009**, *48*, 3080–3086; b) C. Yao, X. Wang, K.-W. Huang, *Chem. Commun.* **2018**, *54*, 3940–3943; c) M. Yadav, A. Metta-Magaña, S. Fortier, *Chem. Sci.* **2020**, *11*, 2381–2387; d) A. K. Maity, J. Murillo, A. J. Metta-Magaña, B. Pinter, S. Fortier, *J. Am. Chem. Soc.* **2017**, *139*, 15691–15700.

[7] a) S. N. Brown, *J. Am. Chem. Soc.* **1999**, *121*, 9752–9753; b) A. G. Maestri, S. D. Taylor, S. M. Schuck, S. N. Brown, *Organometallics* **2004**, *23*, 1932–1946; c) C. Schiller, D. Sieh, N. Lindenmaier, M. Stephan, N. Junker, E. Reijerse, A. A. Granovsky, P. Burger, *J. Am. Chem. Soc.* **2023**, *145*, 11392–11401.

[8] a) M. Wittmer, H. Melchor, *Thin Solid Films* **1982**, *93*, 397–405; b) B. H. Weiller, *J. Am. Chem. Soc.* **1996**, *118*, 4975–4983; c) J. S. Becker, E. Kim, R. G. Gordon, *Chem. Mater.* **2004**, *16*, 3497–3501; d) D. Pilloud, A. S. Dehlinger, J. F. Pierson, A. Roman, L. Pichon, *Surf. Coat. Technol.* **2003**, *174*–*175*, 338–344; e) A. J. Nathanael, R. Yuvakkumar, S. I. Hong, T. H. Oh, *ACS Appl. Mater. Interfaces* **2014**, *10*, 9850–9857; f) S. V. Ushakov, A. Navrotsky, Q.-J. Hong, A. van de Walle, *Materials* **2019**, *12*, 2728–2750.

[9] a) J. Hojo, O. Iwamoto, Y. Maruyama, A. Kato, *J. Less-Common Met.* **1977**, *53*, 265–276; b) Z. Sun, J. Zhang, L. Yin, G. Hu, R. Fang, H.-M. Cheng, F. Li, *Nat. Commun.* **2017**, *8*, 14627; c) Y. Liu, Q. Wu, L. Liu, P. Manasa, L. Kang, F. Ran, *J. Mater. Chem. A* **2020**, *8*, 8218–8233; d) K. Robert, D. Stiévenard, D. Deresmes, C. Douard, A. Iadecola, D. Troadec, P. Simon, N. Nuns, M. Marinova, M. Huvé, P. Roussel, T. Brousse, C. Lethien, *Energy Environ. Sci.* **2020**, *13*, 949–957; e) C. Zhu, P. Yang, D. Chao, X. Wang, X. Zhang, S. Chen, B. K. Tay, H. Huang, H. Zhang, W. Mai, H. J. Fan, *Advanced Materials* **2015**, *27*, 4566–4571; f) B. Gao, X. Li, X. Guo, X. Zhang, X. Peng, L. Wang, J. Fu, P. K. Chu, K. Huo, *Adv. Materials Inter.* **2015**, *2*, 1500211; g) A. Achour, R. Lucio-Porto, M. Chaker, A. Arman, A. Ahmadpourian, M. A. Soussou, M. Boujtita, L. Le Brizoual, M. A. Djouadi, T. Brousse, *Electrochemistry Communications* **2017**, *77*, 40–43; h) A. Kafizas, C. J. Carmalt, I. P. Parkin, *Coordination Chemistry Reviews* **2013**, *257*, 2073–2119; i) T. Nguyen, A. Tavakoli, S. Triqueneaux, R. Swami, A. Ruhtinas, J. Gradel, P. Garcia-Campos, K. Hasselbach, A. Frydman, B. Piot, M. Gibert, E. Collin, O. Bourgeois, *J. Low Temp. Phys.* **2019**, *197*, 348–356.

[10] a) T. Shima, S. Hu, G. Luo, X. Kang, Y. Luo, Z. Hou, *Science* **2013**, *340*, 1549–1552; b) B. Wang, G. Luo, M. Nishiura, S. Hu, T. Shima, Y. Luo, Z. Hou, *J. Am. Chem. Soc.* **2017**, *139*, 1818–1821; c) Z. Mo, T. Shima, Z. Hou, *Angew. Chem. Int. Ed.* **2020**, *59*, 8635–8644; *Angew. Chem.* **2020**, *132*, 8713–8722; d) M. Mena, A. Pérez-Redondo, C. Yélamos, *Eur. J. Inorg. Chem.* **2016**, *2016*, 1762–1778; e) H. W. Roesky, Y. Bai, M. Noltemeyer, *Angew. Chem. Int. Ed. Engl.* **1989**, *28*, 754–755; *Angew. Chem.* **1989**, *101*, 788–789; f) Z. Duan, J. G. Verkade, *Inorg. Chem.* **1996**, *35*, 5325–5327; g) G. Bai, P. Müller, H. W. Roesky, I. Usón, *Organometallics* **2000**, *19*, 4675–4677; h) M. M. B. Holl, P. T. Wolczanski, *J. Am. Chem. Soc.* **1992**, *114*, 3854–3858; i) S. P. Semproni, P. J. Chirik, *J. Am. Chem. Soc.* **2013**, *135*, 11373–11383; j) S. P. Semproni, P. J. Chirik, *Organometallics* **2014**, *33*, 3727–3737; k) D. J. Knobloch, E. Lobkovsky, P. J. Chirik, *J. Am. Chem. Soc.* **2010**, *132*, 10553–10564; l) S. P. Semproni, P. J. Chirik, *Angew. Chem. Int. Ed.* **2013**, *52*, 12965–12969; *Angew. Chem.* **2013**, *125*, 13203–13207; m) D. J. Knobloch, E. Lobkovsky, P. J. Chirik, *Nat. Chem.* **2010**, *2*, 30–35; n) S. P. Semproni, C. Milsmann, P. J. Chirik, *Angew. Chem. Int. Ed.* **2012**, *51*, 5213–5216; *Angew. Chem.* **2012**, *124*, 5303–5306; o) S. P. Semproni, P. J. Chirik, *Organometallics* **2014**, *33*, 3727–3737.

[11] a) G. K. B. Clentsmith, V. M. E. Bates, P. B. Hitchcock, F. G. N. Cloke, *J. Am. Chem. Soc.* **1999**, *121*, 10444–10445; b) M. G. Jafari, D. Fehn, A. Reinholdt, C. Hernández-Prieto, P. Patel, M. R. Gau, P. J. Carroll, J. Krzystek, C. Liu, A. Ozarowski, J. Telser, M. Delferro, K. Meyer, D. J. Mindiola, *J. Am. Chem. Soc.* **2022**, *144*, 10201–10219; c) C. D. Abernethy, F. Bottomley, A. Decken, T. S. Cameron, *Organometallics* **1996**, *15*, 1758–1759; d) A. J. Keane, B. L. Yonke, M. Hirotsu, P. Y. Zavalij, L. R. Sita, *J. Am. Chem. Soc.* **2014**, *136*, 9906–9909; e) F. Akagi, T. Matsuo, H. Kawaguchi, *Angew. Chem. Int. Ed.* **2007**, *46*, 8778–8781; *Angew. Chem.* **2007**, *119*, 8934–8937; f) K. Searles, P. J. Carroll, C.-H.

RESEARCH ARTICLE

Chen, M. Pink, D. J. Mindiola, *Chem. Commun.* **2015**, *51*, 3526–3528; g) A. Caselli, E. Solari, R. Scopelliti, C. Floriani, N. Re, C. Rizzoli, A. Chiesi-Villa, *J. Am. Chem. Soc.* **2000**, *122*, 3652–3670; h) M. D. Fryzuk, C. M. Kozak, M. R. Bowdridge, B. O. Patrick, S. J. Rettig, *J. Am. Chem. Soc.* **2002**, *124*, 8389–8397; i) A. J. Keane, P. Y. Zavalij, L. R. Sita, *J. Am. Chem. Soc.* **2013**, *135*, 9580–9583.

[12] a) F. Akagi, T. Matsuo, H. Kawaguchi, *Angew. Chem. Int. Ed.* **2007**, *46*, 8778–8781; *Angew. Chem.* **2007**, *119*, 8934–8937; b) J. J. Curley, A. F. Cozzolino, C. C. Cummins, *Dalton Trans.* **2011**, *40*, 2429–2432; c) E. L. Sceats, J. S. Figueiroa, C. C. Cummins, N. M. Loening, P. Van der Wel, R. G. Griffin, *Polyhedron* **2004**, *23*, 2751–2768; d) T. Agapie, A. L. Odom, C. C. Cummins, *Inorg. Chem.* **2000**, *39*, 174–179; e) C. C. Cummins, *Angew. Chem. Int. Ed.* **2006**, *45*, 862–870; f) F. Akagi, S. Suzuki, Y. Ishida, T. Hatanaka, T. Matsuo, H. Kawaguchi, *Eur. J. Inorg. Chem.* **2013**, *2013*, 3930–3936; g) J. K. Brask, V. Durà-Vilà, P. L. Diaconescu, C. C. Cummins, *Chem. Commun.* **2002**, 902–903; h) C. R. Clough, J. B. Greco, J. S. Figueiroa, P. L. Diaconescu, W. M. Davis, C. C. Cummins, *J. Am. Chem. Soc.* **2004**, *126*, 7742–7743; i) L. M. Duman, W. S. Farrell, P. Y. Zavalij, L. R. Sita, *J. Am. Chem. Soc.* **2016**, *138*, 14856–14859; j) J. S. Figueiroa, N. A. Piro, C. R. Clough, C. C. Cummins, *J. Am. Chem. Soc.* **2006**, *128*, 940–950; k) Y. Ishida, H. Kawaguchi, in *Nitrogen Fixation* (Ed.: Y. Nishibayashi), Springer International Publishing, Cham, **2017**, pp. 45–69; l) D. J. Mindiola, C. C. Cummins, *Angew. Chem. Int. Ed.* **1998**, *37*, 945–947; *Angew. Chem.* **1998**, *110*, 983–986; m) D. J. Mindiola, K. Meyer, J.-P. F. Cherry, T. A. Baker, C. C. Cummins, *Organometallics* **2000**, *19*, 1622–1624; n) J. S. Silvia, C. C. Cummins, *J. Am. Chem. Soc.* **2010**, *132*, 2169–2171.

[13] a) G. A. Silantyev, M. Färster, B. Schluschaß, J. Abbenseth, C. Wgrtele, C. Volkmann, M. C. Holthausen, S. Schneider, *Angew. Chem. Int. Ed.* **2017**, *56*, 5872–5876; *Angew. Chem.* **2017**, *129*, 5966–5970; b) J. R. Dilworth, P. L. Dahlstrom, J. R. Hyde, J. Zubieto, *Inorg. Chim. Acta* **1983**, *71*, 21–28; c) M. B. O'Donoghue, W. M. Davis, R. R. Schrock, *Inorg. Chem.* **1998**, *37*, 5149–5158; d) T. Miyazaki, H. Tanaka, Y. Tanabe, M. Yuki, K. Nakajima, K. Yoshizawa, Y. Nishibayashi, *Angew. Chem. Int. Ed.* **2014**, *53*, 11488–11492; *Angew. Chem.* **2014**, *126*, 11672–11676; e) H. Tanaka, K. Arashiba, S. Kuriyama, A. Sasada, K. Nakajima, K. Yoshizawa, Y. Nishibayashi, *Nat. Commun.* **2014**, *5*, 3737–3747; f) M. G. Fickes, A. L. Odom, C. C. Cummins, *Chem. Commun.* **1997**, 1993–1994.

[14] a) R. Thompson, C.-H. Chen, M. Pink, G. Wu, D. J. Mindiola, *J. Am. Chem. Soc.* **2014**, *136*, 8197–8200; b) M. E. Carroll, B. Pinter, P. J. Carroll, D. J. Mindiola, *J. Am. Chem. Soc.* **2015**, *137*, 8884–8887.

[15] a) L. N. Grant, B. Pinter, J. Gu, D. J. Mindiola, *J. Am. Chem. Soc.* **2018**, *140*, 17399–17403; b) M. Bhunia, C. Sandoval-Pauker, M. G. Jafari, L. N. Grant, M. R. Gau, B. Pinter, D. J. Mindiola, *Angew. Chem. Int. Ed.* **2022**, *61*, e202209122; *Angew. Chem.* **2022**, *134*, e202209122.

[16] L. N. Grant, B. Pinter, T. Kurogi, M. E. Carroll, G. Wu, B. C. Manor, P. J. Carroll, D. J. Mindiola, *Chem. Sci.* **2017**, *8*, 1209–1224.

[17] See the supporting information for details.

[18] Deposition numbers 2332762 (2), 2332765 (3), 2178167 (4), 2178168 (5), 2332764 (6), 2178169 (7), 2332766 (8), 2332763 (9), and 2332767 (13) contain the supplementary crystallographic data. These data are provided free of charge by the joint Cambridge Crystallographic Data Centre and Fachinformationszentrum Karlsruhe Access Structures service.

[19] Z.-J. Lv, P. D. Engel, L. Alig, S. Maji, M. C. Holthausen, S. Schneider, *J. Am. Chem. Soc.* **2022**, *144*, 21872–21877.

[20] a) H. Asakawa, K.-H. Lee, Z. Lin, M. Yamashita, *Nat. Commun.* **2014**, *5*, 4245; b) M. Xu, B. Kooij, T. Wang, J. H. Lin, Z. Qu, S. Grimme, D. W. Stephan, *Angew. Chem. Int. Ed.* **2021**, *60*, 16965–16969; *Angew. Chem.* **2021**, *133*, 17102–17106.

[21] a) J. L. Dye, *Science* **2003**, *301*, 607–608; b) A. S. Ichimura, M. J. Wagner, J. L. Dye, *J. Phys. Chem. B* **2002**, *106*, 11196–11202.

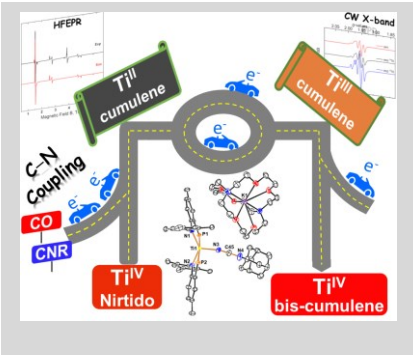
[22] J. Krzystek, A. Ozarowski, J. Telser, *Coordination Chemistry Reviews* **2006**, *250*, 2308–2324.

[23] M. Bhunia, J. S. Mohar, C. Sandoval-Pauker, D. Fehn, E. S. Yang, M. Gau, J. Goicoechea, A. Ozarowski, J. Krzystek, J. Telser, K. Meyer, D. J. Mindiola, *J. Am. Chem. Soc.* **2024**, *146*, 3609–3614.

RESEARCH ARTICLE

Article

A titanium nitride undergoes N-C bond coupling with carbon monoxide and isocyanides to form Ti^{II} cumulene complexes $[(PN)_2Ti(NCE)]^-$ ($E = O, NAd, N'Bu$). Oxidation of these affords the Ti^{III} cumulene $[(PN)_2Ti(NCE)]$. Further oxidation affords a Ti^{IV} bis-cumulene *trans*- $[(PN)_2Ti(NCNAd)_2]$. Structural, electrochemical, and spectroscopic studies (HFEPR, CW X-band, NMR and IR spectroscopies), including ^{15}N isotopic labelling studies are presented and discussed to understand the bonding and topology.



M. Bhunia, C. Sandoval-Pauker, D. Fehn, L. N. Grant, S. Senthil, M. R. Gau, A. Ozarowski, J. Krzystek, J. Telser,* B. Pinter,* K. Meyer,* and D. J. Mindiola*

Divalent Titanium via Reductive N-C Coupling of a Ti^{IV} Nitrido with π -Acids.

Twitter Account:
@MindiolaGroup
@MrinalBhunia